The Plant Cell, Vol. 26: 2007–2023, May 2014, www.plantcell.org

Spatiotemporal Production of Reactive Oxygen Species by NADPH Oxidase Is Critical for Tapetal Programmed Cell Death and Pollen Development in *Arabidopsis*[C][W]

Hong-Tao Xie, Zhi-Yuan Wan, Sha Li, and Yan Zhang[1]

State Key Laboratory of Crop Biology, College of Life Sciences, Shandong Agricultural University, Tai'an 271018, China

ORCID ID: 0000-0002-3501-5857 (Y.Z.)

Male sterility in angiosperms has wide applications in agriculture, particularly in hybrid crop breeding and gene flow control. Microspores develop adjacent to the tapetum, a layer of cells that provides nutrients for pollen development and materials for pollen wall formation. Proper pollen development requires programmed cell death (PCD) of the tapetum, which requires transcriptional cascades and proteolytic enzymes. Reactive oxygen species (ROS) also affect tapetal PCD, and failures in ROS scavenging cause male sterility. However, many aspects of tapetal PCD remain unclear, including what sources generate ROS, whether ROS production has a temporal pattern, and how the ROS-producing system interacts with the tapetal transcriptional network. We report here that stage-specific expression of NADPH oxidases in the *Arabidopsis thaliana* tapetum contributes to a temporal peak of ROS production. Genetic interference with the temporal ROS pattern, by manipulating *RESPIRATORY-BURST OXIDASE HOMOLOG* (*RBOH*) genes, affected the timing of tapetal PCD and resulted in aborted male gametophytes. We further show that the tapetal transcriptional network regulates *RBOH* expression, indicating that the temporal pattern of ROS production intimately connects to other signaling pathways regulated by the tapetal transcriptional network to ensure the proper timing of tapetal PCD.

INTRODUCTION

The control of male fertility in angiosperms has attracted wide attention in the past decades due to its vital importance for crop breeding, hybrid production, and gene flow control for transgenes (Wilson and Zhang, 2009). Extensive studies have shown that the finely tuned process of male gametophytic development requires contributions by and collaborations from the surrounding sporophytic cells (Wilson and Zhang, 2009; Parish and Li, 2010; Chang et al., 2011). Microsporocytes in anther locules are surrounded by four somatic cell layers, the epidermis, endothecium, middle layer, and tapetum, during stages 1 to 5 in *Arabidopsis thaliana* (Sanders et al., 1999) or stages 1 to 6 in rice (*Oryza sativa*) (Zhang et al., 2011). Tapetal cells develop adjacent to microspores. Following the completion of meiosis, tapetal cells play a crucial role in microsporogenesis by supplying proteins, lipids, and pigments, first through secretion and later through degradation (Parish and Li, 2010). In *Arabidopsis*, visible tapetal degeneration starts at stage 10 and lasts to stage 11, when pollen mitotic division occurs (Sanders et al., 1999; Parish and Li, 2010). This differs slightly from rice, in which tapetal degeneration was detected as early as the tetrad stage (Zhang et al., 2011).

The production of viable pollen requires the proper timing of tapetal degradation, which occurs via developmentally regulated programmed cell death (PCD). Tapetal PCD is tightly controlled by evolutionarily conserved transcriptional cascades (Wilson and Zhang, 2009; Parish and Li, 2010; Ma et al., 2012). In *Arabidopsis*, spatiotemporal expression of genes encoding transcription factors controls tapetal function (Wilson and Zhang, 2009; Parish and Li, 2010; Chang et al., 2011; Zhu et al., 2011). Mutations of these genes, such as *DYSFUNCTIONAL TAPETUM1* (*DYT1*) (Zhang et al., 2006), *DEFECTIVE IN TAPETAL DEVELOPMENT AND FUNCTION1* (*TDF1*/*MYB35*) (Feng et al., 2012), *MYB33* and *MYB65* (Millar and Gubler, 2005), *ABORTED MICROSPORES* (*AMS*) (Xu et al., 2010), *MYB80* (also known as *MYB103*) (Higginson et al., 2003; Zhang et al., 2007; Phan et al., 2011), and *MALE STERILITY1* (*MS1*) (Wilson et al., 2001; Vizcay-Barrena and Wilson, 2006; Ito et al., 2007; Yang et al., 2007), all led to pollen abortion and male sterility. Elegant transcriptomic (Xu et al., 2010; Feng et al., 2012; Ma et al., 2012) and genetic (Zhu et al., 2011) studies integrated these key transcription factors into a transcriptional network regulating tapetal PCD, in which linear as well as complex interactions among these transcription factors may be delicately intertwined to ensure the proper timing of tapetal PCD (Zhu et al., 2011; Ma et al., 2012). Most components in the *Arabidopsis* tapetal transcriptional network have functional counterparts in rice (Li et al., 2006; Zhang et al., 2008; Li et al., 2011; Phan et al., 2012; Niu et al., 2013), suggesting its evolutionary conservation.

Genes encoding proteolytic enzymes are often targets of the tapetal transcriptional network (Li et al., 2006; Phan et al., 2011; Niu et al., 2013). Mutations of rice *TAPETUM DEGENERATION RETARDATION* (*TDR*), a counterpart of *Arabidopsis AMS* (Li et al., 2006; Zhang et al., 2008), resulted in delayed tapetal PCD and pollen abortion (Li et al., 2006; Zhang et al., 2008).

[1] Address correspondence to yzhang@sdau.edu.cn.
The author responsible for distribution of materials integral to the findings presented in this article in accordance with the policy described in the Instructions for Authors (www.plantcell.org) is: Yan Zhang (yzhang@sdau.edu.cn).
[C] Some figures in this article are displayed in color online but in black and white in the print edition.
[W] Online version contains Web-only data.
www.plantcell.org/cgi/doi/10.1105/tpc.114.125427

Interestingly, genes encoding a Cys protease and a protease inhibitor are likely targeted by TDR (Li et al., 2006). Rice *ETERNAL TAPETUM1*, operating downstream of TDR, was recently found to regulate the expression of two aspartic proteases, both of which promoted PCD (Niu et al., 2013). In *Arabidopsis*, genome-wide transcriptomic analyses identified several Cys protease–encoding genes as potential targets of MS1 (Yang et al., 2007). Indeed, a direct target of MYB80, *UNDEAD*, encodes an A1 aspartic protease whose functional loss resulted in premature tapetal PCD (Phan et al., 2011). These data support the existence of a protease-mediated pathway for the execution of plant developmental PCD (Lam, 2004).

Another universal theme in developmental PCD is the involvement of reactive oxygen species (ROS) (Beers and McDowell, 2001; Lam, 2004; Gechev et al., 2006; De Pinto et al., 2012). ROS, such as superoxide and hydrogen peroxide, are critical signaling molecules affecting a large number of proteins through posttranslational modifications, transcriptional changes, or activity changes (Neill et al., 2002; Lam, 2004; Mittler et al., 2004, 2011; Torres and Dangl, 2005; Suzuki et al., 2011). It was shown that rice anthers display ROS levels that increase until stages 8 and 9 and then decrease to complete absence at stage 11 (Hu et al., 2011). This temporal change of ROS was abolished in *mads3* mutant anthers, in which tapetal PCD occurs prematurely (Hu et al., 2011). One target of MADS3 is *MT-1-4b*, encoding a protein with ROS-scavenging activity in vitro (Hu et al., 2011). Also, the determining factor of rice wild abortive cytoplasmic male sterility encodes a tapetal mitochondrial protein, WA352, whose interaction with the nucleus-encoded mitochondrial protein COX11 inhibits its ROS-scavenging activity, resulting in premature tapetal PCD and pollen abortion (Luo et al., 2013).

Although these data hinted at the involvement of ROS in tapetal PCD (Hu et al., 2011; Luo et al., 2013), it remains unclear how ROS are generated, whether ROS production undergoes temporal changes in the tapetum, and how the ROS-producing system interacts with the tapetal transcriptional network. We report here that tapetal PCD requires temporal control of ROS levels by the spatiotemporal expression of *RESPIRATORY-BURST OXIDASE HOMOLOG* (*RBOH*) genes. *RBOH*s encode NADPH oxidases that localize at the plasma membrane to produce O_2^-, which then mostly converts to apoplastic H_2O_2 (Keller et al., 1998; Torres and Dangl, 2005; Marino et al., 2012). *RBOH*s play crucial roles in cell growth, development, and abiotic and biotic stress responses (Suzuki et al., 2011; Marino et al., 2012; Lee et al., 2013). Our work indicates that the temporal ROS pattern produced by NADPH oxidases, together with other signaling pathways, is under complex control of the tapetal transcriptional network to ensure the proper timing of tapetal PCD.

RESULTS

Spatiotemporal Expression of *RBOHE*

The *Arabidopsis* genome encodes 10 *RBOH*s. We identified *RBOHE* (At1g19230) as an anther-preferential or tapetum-enriched gene by mining several microarray studies of the tapetal transcriptome (Wijeratne et al., 2007; Feng et al., 2012; Ma et al., 2012). To verify the tapetum-enriched expression of *RBOHE*, we generated more than 20 individual Pro_{RBOHE}:GUS (for β-glucuronidase) reporter lines and analyzed GUS expression by histochemical analysis. The Pro_{RBOHE}:GUS transgenic anthers showed GUS signals in the tapetal layer during anther developmental stages 6 to 11 (Figure 1A), a spatiotemporal expression pattern confirmed by RNA in situ analysis (Figures 1B to 1D). These lines of evidence demonstrated the temporal expression of *RBOHE* in tapetum, implying its involvement in late tapetal function.

Functional Loss of *RBOHE* Resulted in Sporophytic Male Defects

The spatiotemporal expression of *RBOHE* in tapetum suggested its involvement in pollen development. To test this, we characterized two T-DNA insertion mutants of *RBOHE*, *rbohe-1* and *rbohe-2*. No transcript was detectable by RT-PCR in *rbohe-1* and *rbohe-2* mutants using gene-specific primers flanking the insertion sites (Figures 2A and 2B) or by RNA in situ hybridization in *rbohe-1* (Figure 1D), supporting the idea that these are null alleles for *RBOHE*. F1 plants generated from crosses between *rbohe-1* and *rbohe-2* showed similar pollen developmental defects to either parent (Supplemental Figure 1), indicating that they are allelic. However, *rbohe-1* contains another insertion that caused a long-petiole phenotype. Thus, *rbohe-2* was analyzed in detail and used to generate double mutants in the following studies, unless noted otherwise.

A substantial portion of pollen grains from both mutants aborted, as judged by scanning electron microscopy (Figures 2C to 2H) and Alexander dye staining (Supplemental Figure 1). Scanning electron microscopy of mature pollen (Figures 2C to 2H) showed that, unlike the well-organized reticular exine structure of wild-type pollen (Figures 2C and 2F), mutant pollen showed irregular exine patterns and a deformed shape (Figures 2D, 2E, 2G, and 2H). Further examination by transmission electron microscopy (Figures 2I to 2L) confirmed the pollen developmental defects in the *RBOHE* loss-of-function mutants. Wild-type pollen showed a layered structure with intine, nexine, sexine, and pollen coat from inner to outer layers (Figures 2I and 2K). A substantial portion of mutant pollen grains contained intact intine but hardly any nexine structure (Figures 2J and 2L). Both pollen coat and sexine structure were nearly absent in the mutant pollen (Figures 2J and 2L). As a result of the significantly increased pollen abortion rates, *RBOHE* loss of function resulted in partial sterility (Supplemental Figure 1).

To find out whether the defective pollen development was sporophytic or gametophytic, we first analyzed pollen from heterozygous mutants of *RBOHE* and found that they have a normal pollen coat (Supplemental Figure 1). Pollen germination of *RBOHE* heterozygous mutants was comparable to that of the wild type but significantly reduced in its homozygous mutants (Supplemental Figure 1), confirming that *RBOHE* loss of function resulted in sporophytic rather than gametophytic male defects.

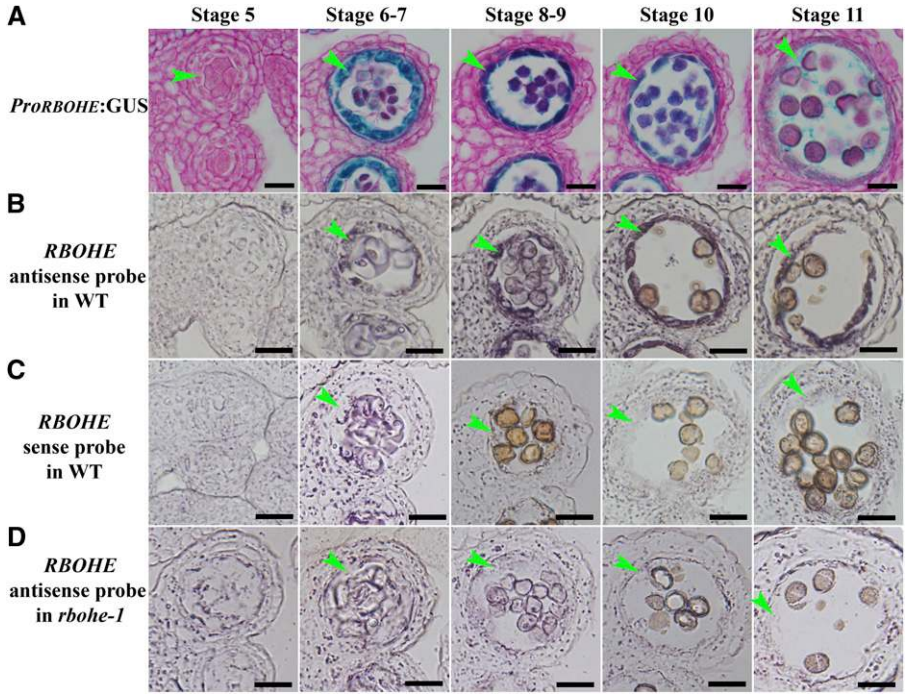

Figure 1. Expression of *RBOHE* in the Tapetum during Anther Stages 6 to 11.

(A) Histochemical staining of representative anther sections from Pro_{RBOHE}:GUS transgenic plants at different developmental stages.
(B) to **(D)** RNA in situ analyses of *RBOHE* expression at different developmental stages using an antisense probe either in the wild type **(B)** or in *rbohe-1* **(D)**. Wild-type anthers at corresponding stages were incubated with a sense probe as controls **(C)**. Arrowheads point to the tapetal layer.
Bars = 20 μm.

Functional Loss of *RBOHE* Resulted in Delayed Tapetal Degeneration

Because the spatiotemporal expression of *RBOHE* occurred at the same time as tapetal degeneration (Phan et al., 2011) and functional loss of *RBOHE* resulted in pollen abortion (Figure 2), we wondered whether the sporophytic defects in *RBOHE* loss-of-function mutants were due to defective tapetal degeneration.

To test this hypothesis, we first aimed at identifying the developmental defects of *rbohe-2* by histological analyses. We compared transverse semithin sections of developing wild-type and *rbohe-2* anthers from stages 6 to 12. The tapetum of *rbohe-2* (Figure 3F) was morphologically comparable to that of the wild type at stages 6 and 7 (Figure 3A). However, *rbohe-2* tapetum remained highly densely stained (Figure 3G) at stage 8, when wild-type tapetal cells began to shrink (Figure 3B). The middle layer persisted in *rbohe-2* (Figure 3G), but it largely disappeared in the wild type (Figure 3B). Wild-type tapetum gradually degenerated into a thin and broken layer at stage 11 (Figures 3C and 3D) and disappeared completely at stage 12 (Figure 3E), accompanied by septum breakage (Figure 3E). By contrast, *rbohe-2* tapetum remained intact and became slightly hypertrophic until stage 11 (Figures 3H and 3I). At stage 12, a thin and broken layer of tapetum was still visible in *rbohe-2* (Figure 3J). These histological analyses indicated a delayed degeneration of tapetal cells in *rbohe-2*.

To find out more cytosolic details of the effects of *RBOHE* loss of function on the tapetal cells, we performed transmission electron microscopy on mutant anthers at late developmental stages. Consistent with the results of histological analyses, *rbohe-2* mutants showed delayed tapetal degeneration. Microspores form an exine wall in the wild type at stage 9 (Figure 3K). Tapetal cells of the wild type at this stage accumulate numerous tapetosomes and elaioplasts (Hsieh and Huang, 2007), which eventually deposit their contents to developing microspores (Figure 3K). By contrast, *rbohe-2* at the same stage contained a thicker tapetal layer (Figure 3N). At stage 11, wild-type tapetal cells degenerated, with disintegrated cellular organization (Figures 3L and 3M). By contrast, tapetal cells of *rbohe-2* remained intact and contained numerous tapetosomes and elaioplasts, which failed to release into anther locules (Figures 3O and 3P). The development of microspores was significantly retarded in *rbohe-2* (Figure 3O) as compared with that in the wild type (Figure 3L), confirming delayed tapetal degradation in *rbohe-2*.

Functional Redundancy in Pollen Development by *RHD2*

Despite the clear effect of *RBOHE* loss of function in tapetal degeneration, we wondered whether another *RBOH* functioned redundantly with *RBOHE*, as reported for other processes (Torres et al., 2002; Kwak et al., 2003). Close examination of anther transcriptomic data (Wijeratne et al., 2007) indicated that *RHD2*, also named *RBOHC*, which belongs to the same *RBOH* family (Torres and Dangl, 2005), was possibly also a tapetal gene, despite its involvement in root hair growth (Foreman et al., 2003).

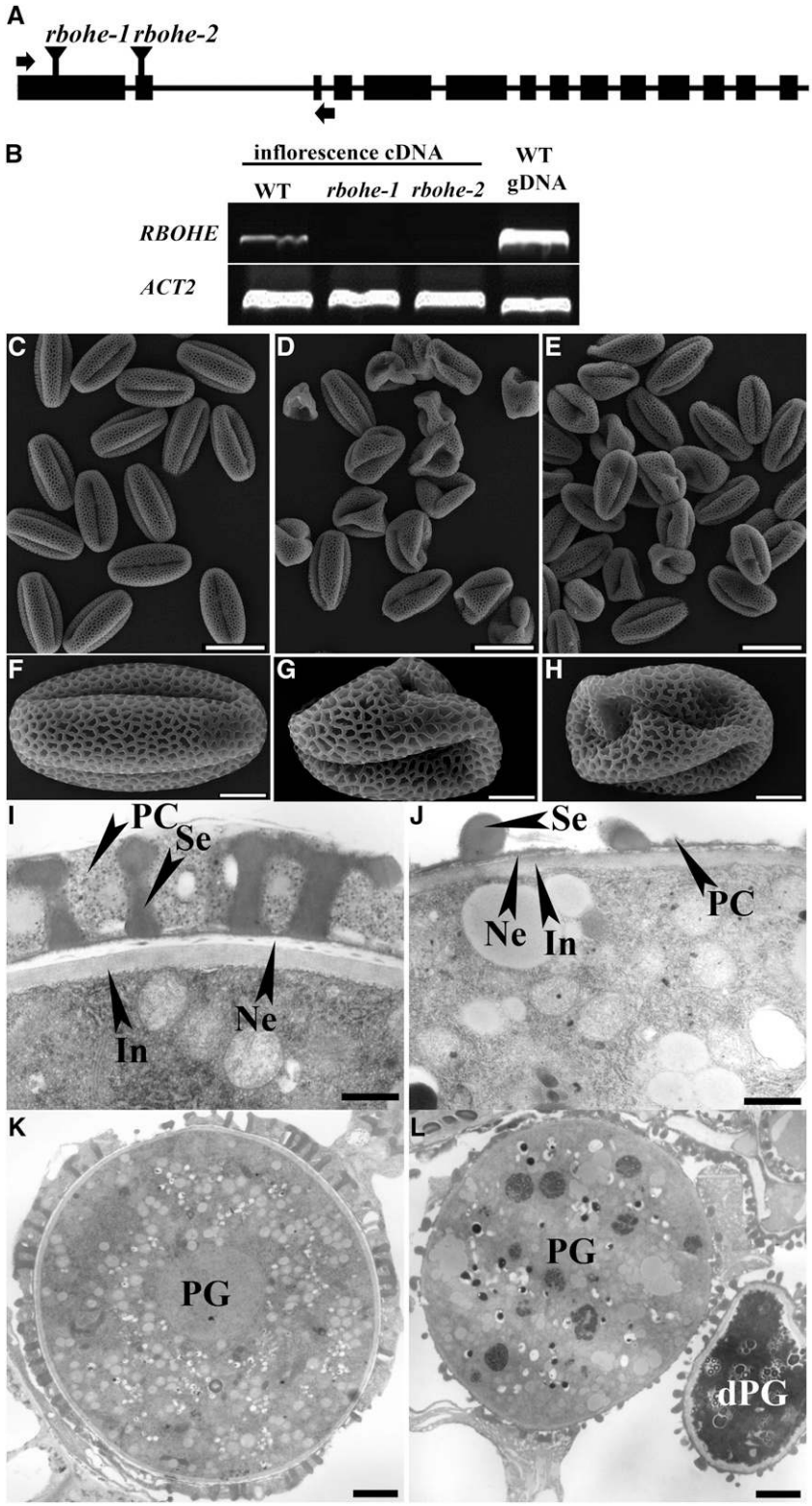

Figure 2. Functional Loss of *RBOHE* Resulted in Pollen Developmental Defects.

(A) Schematic illustration of T-DNA insertions within the *RBOHE* genomic region. Arrows indicate the binding sites of primers used for RT-PCR.

To find out whether *RHD2* was expressed in the tapetum, we performed RNA in situ hybridization in anthers of various developmental stages (Supplemental Figure 2). Positive signals were detected in tapetum from stages 6 to 10 (Supplemental Figure 2). We also generated promoter:GUS reporter lines for *RHD2*. Histochemical analyses of Pro_{RHD2}:GUS transgenic anthers confirmed the spatiotemporal expression of *RHD2* by RNA in situ hybridization (Supplemental Figure 2). We note, however, that under the same analytical conditions, the expression level of *RHD2* was much lower than that of *RBOHE* in the tapetum, suggesting a minor role of *RHD2*.

To test whether *RHD2* was redundant with *RBOHE* in tapetum, we generated the *rbohe-2 rhd2-1* double mutant by crossing *rbohe-2* with *rhd2-1*, described previously as a null mutant for *RHD2* (Foreman et al., 2003). Compared with the wild type (Figures 4A, 4D, and 4G), functional loss of *RHD2* did not affect pollen development significantly (Figures 4B, 4E, and 4H; Supplemental Figure 1). In *rbohe-2 rhd2-1*, however, pollen development was severely compromised (Figures 4C, 4F, and 4I). More of the pollen appeared to be deformed in the double mutants, leading to significantly reduced fertility (Figure 4F; Supplemental Figure 1). The tapetum in the double mutant was comparably normal before stage 7 (Figures 4J and 4K). However, densely stained tapetal cells persisted in the double mutant until stage 12 (Figures 4L to 4P). Only at stage 13, when septum and stomium degenerated to break the anther wall, did the tapetal layer disappear in *rbohe-2 rhd2-1* mutants (Figure 4Q). The middle layer disappeared at stage 8 in the wild type (Figure 3C) but was still visible in the double mutant even at stage 13 (Figure 4Q), likely a secondary effect of defective tapetal degeneration. These results showed that *RHD2* plays a redundant, albeit minor, role in tapetal degeneration and pollen development compared with *RBOHE*.

Overexpression of *RBOHE* Resulted in Precocious Tapetal Degeneration

To explore the possibility that the spatiotemporal *RBOHE* expression was crucial for tapetal degeneration and pollen development, we attempted to manipulate *RBOHE* levels by overexpressing *RBOHE*. *RBOHE* has two annotated splicing variants, and we cloned a novel *RBOHE* splicing form (*RBOHE.3*) by using anther cDNA libraries as a template for PCR (Supplemental Figure 3). *RBOHE.3* potentially encodes an RBOHE with intact enzymatic sites, similar to other variants (Supplemental Figure 3). To prove that RBOHE.3 has NADPH oxidase function, we used a tobacco (*Nicotiana benthamiana*) infiltration system to examine its in vitro activity (Supplemental Figure 3). Nitrotetrazolium blue chloride (NBT) staining of tobacco leaves expressing RBOHE.3 showed enhanced ROS production, whereas leaves expressing a C-terminal truncated RBOHE.3 that lacks its enzymatic domains and leaves expressing the empty vector did not show enhanced ROS production (Supplemental Figure 3), indicating that *RBOHE.3* encodes a functional NADPH oxidase.

To manipulate the expression level of *RBOHE*, we used the rice promoter Pro_{Osg6B} (Tsuchiya et al., 1994; Kawanabe et al., 2006), which is active in the tapetum from stages 6 to 10 (Figure 5A). We generated 35 transgenic lines expressing *RBOHE.3* driven by Pro_{Osg6B}, among which 27 individual transgenic lines (OX-S1 to OX-S27) showed complete pollen abortion and complete sterility, while eight individual transgenic lines (OX-M1 to OX-M8) showed significantly increased pollen abortion (Supplemental Figure 4). Two representative transgenic lines, OX-M1 for medium overexpression and OX-S1 for strong overexpression, were chosen for further studies based on transcript analyses that correlate *RBOHE* expression with pollen abortion rates (Supplemental Figure 4).

Histological analyses of tapetal cells in developing anthers showed that Pro_{Osg6B}:RBOHE anthers were indistinguishable from those of the wild type before anther stage 6 (Figure 5B). However, starting from anther stage 7 after tetrads were released into anther locules (Figure 5B), tapetal cells were densely stained in Pro_{Osg6B}:RBOHE anthers (Figure 5B). In addition to lightly stained microspores, anther locules were filled with cellular debris (Figure 5B), suggesting cellular disintegration. At stage 9, the tapetal layer of Pro_{Osg6B}:RBOHE anthers was hardly recognizable, with more cellular debris filling anther locules (Figure 5B). At stage 10, microspores were highly vacuolated and mostly degenerated (Figure 5B). Pro_{Osg6B}:RBOHE anther locules were finally empty, with only degenerating microspores, at stage 11 (Figure 5B). By transmission electron microscopy, we found that, unlike the tapetal cells of the wild type, which showed a clear cell wall structure at stages 8 and 9 (Figure 3K) and partially degenerated tapetal cells at stage 11 (Figure 3M), no cell wall structure was detected in the tapetal layer of Pro_{Osg6B}:RBOHE anthers (Figure 5C). In addition, overexpression of *RBOHE* caused early degeneration of tapetal cells such that the tapetal layer was not present at stage 10 (Figure 5C). In addition, microspores degenerated as early as at stage 9 in Pro_{Osg6B}:RBOHE anthers (Figure 5C), likely due to dysfunction of the tapetum. These results suggested that overexpressing *RBOHE* induced precocious tapetal degeneration (Figure 5C).

Figure 2. (continued).

(B) Transcript analysis by RT-PCR showing the loss of *RBOHE* expression in both mutant alleles. *ACTIN2* (*ACT2*) was used as the internal control. gDNA, genomic DNA.

(C) to **(E)** Scanning electron micrographs of pollen grains from the wild type **(C)**, *rbohe-1* **(D)**, and *rbohe-2* **(E)**.

(F) to **(H)** Scanning electron micrographs of a single pollen grain from the wild type **(F)**, *rbohe-1* **(G)**, and *rbohe-2* **(H)**.

(I) to **(L)** Transmission electron micrographs of pollen from stage 11 anthers of the wild type (**[I]** and **[K]**) or *rbohe-2* (**[J]** and **[L]**). dPG, degenerated pollen grain; In, intine; Ne, nexine; PC, pollen coat; PG, pollen grains; Se, sexine.

Bars in **(C)** to **(E)** = 20 μm; bars in **(F)** to **(H)** = 5 μm; bars in **(I)** and **(J)** = 500 nm; bars in **(K)** and **(L)** = 2 μm.

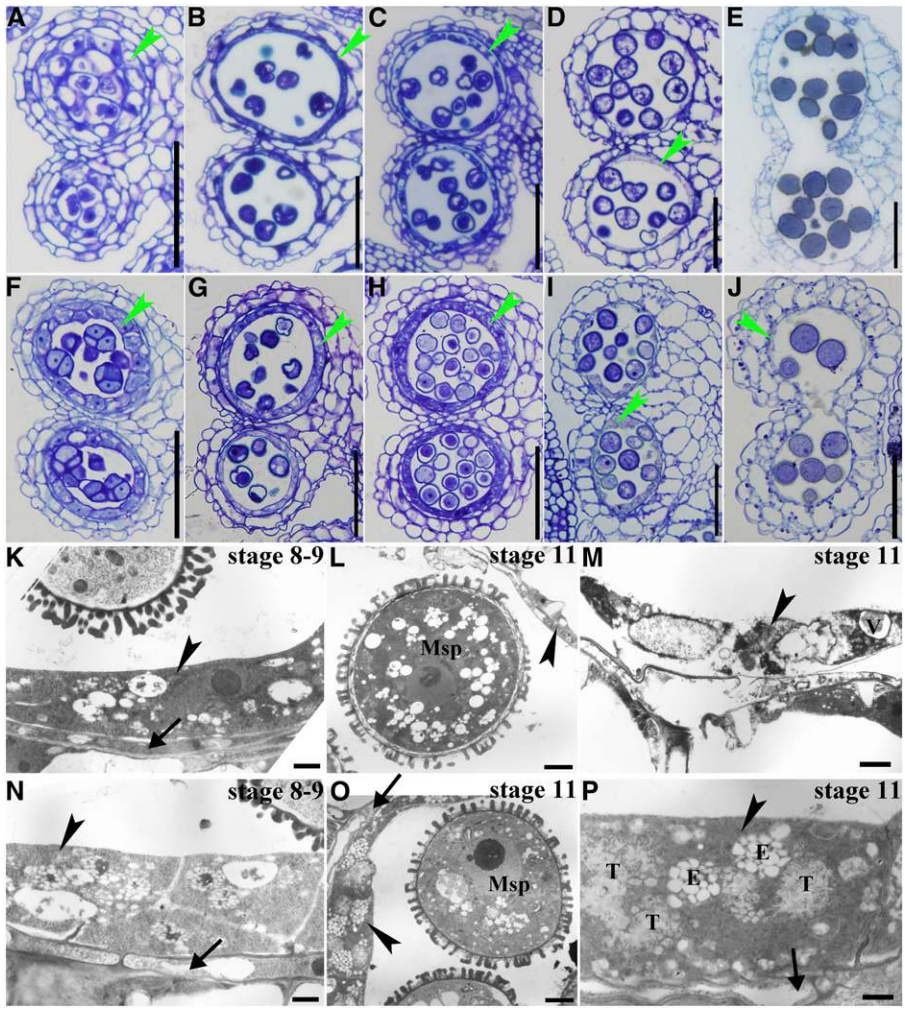

Figure 3. Functional Loss of *RBOHE* Resulted in Delayed Tapetal Degeneration.

(A) to **(E)** Transverse semithin sections of wild-type anthers at developmental stages 6 and 7 **(A)**, stages 8 and 9 **(B)**, stage 10 **(C)**, stage 11 **(D)**, and stage 12 **(E)**.
(F) to **(J)** Transverse semithin sections of *rbohe-2* anthers at developmental stages 6 and 7 **(F)**, stages 8 and 9 **(G)**, stage 10 **(H)**, stage 11 **(I)**, and stage 12 **(J)**.
Arrowheads point to the tapetal layer.
(K) to **(M)** Transmission electron micrographs of wild-type anthers at anther stages 8 and 9 **(K)** or stage 11 (**[L]** and **[M]**).
(N) to **(P)** Transmission electron micrographs of *rbohe-2* anthers at anther stages 8 and 9 **(N)** or stage 11 (**[O]** and **[P]**).
Arrows point to the middle layer, which was not observed in stage 11 wild type (**[L]** and **[M]**) but persisted in stage 11 *rbohe-2* anthers (**[O]** and **[P]**).
Arrowheads point to the tapetal layer. E, elaioplast; Msp, microspore; T, tapetosome; V, vacuole.
Bars in **(A)** to **(J)** = 50 μm; bars in **(K)**, **(M)**, **(N)**, and **(P)** = 1 μm; bars in **(L)** and **(O)** = 2 μm.
[See online article for color version of this figure.]

RBOHE Loss or Gain of Function Interfered with the Timing of Tapetal PCD

To find out whether the delayed or precocious tapetal degeneration reflected the different timing of tapetal PCD, we performed terminal deoxynucleotidyl transferase–mediated dUTP nick-end labeling (TUNEL) assays on *RBOHE* loss- or gain-of-function anthers, in which positive signals indicate cells undergoing massive DNA fragmentation.

As reported previously (Vizcay-Barrena and Wilson, 2006; Phan et al., 2011), no TUNEL-positive signal could be detected in the wild type before stage 10 (Figure 6A). At stage 10, tapetal cells underwent PCD, leading to TUNEL-positive signals (Figure 6A). At stage 11, not only tapetal cells but also septum cells degenerated to produce TUNEL-positive signals (Figure 6A). By contrast, no TUNEL-positive signals could be detected at stage 10 or before in *rbohe-2* (Figure 6B). Only at stage 11, when vascular and septum cells degenerated, did TUNEL-positive

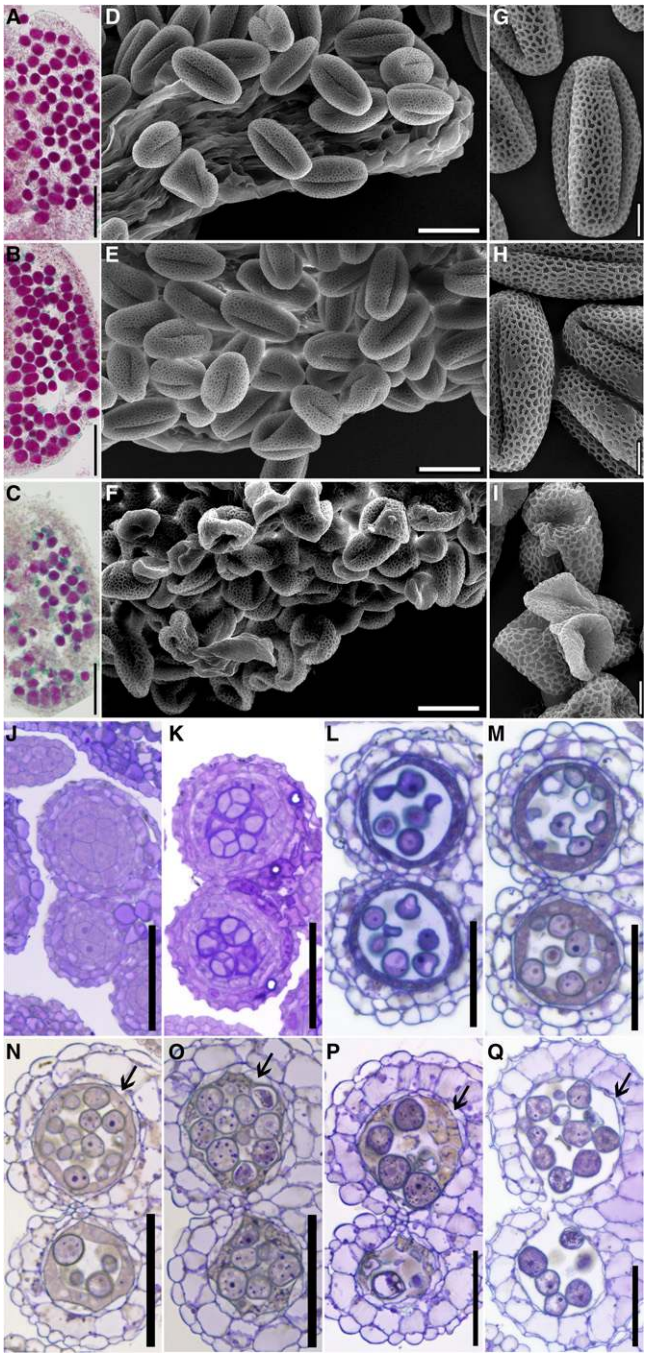

Figure 4. *RHD2*/*RBOHC* Confers Functional Redundancy to *RBOHE* in Pollen Development.

(A) to **(C)** Alexander dye staining of mature anthers from the wild type **(A)**, *rhd2-1* **(B)**, and *rbohe-2 rhd2-1* **(C)**.

(D) to **(F)** Scanning electron micrographs of dehiscing anthers from the wild type **(D)**, *rhd2-1* **(E)**, and *rbohe-2 rhd2-1* **(F)**.

(G) to **(I)** Scanning electron micrographs of pollen grains from the wild type **(G)**, *rhd2-1* **(H)**, and *rbohe-2 rhd2-1* **(I)**.

(J) to **(Q)** Transverse semithin sections of *rbohe-2 rhd2-1* anthers at stages 5 and 6 **(J)**, stage 7 **(K)**, stage 8 **(L)**, stage 9 **(M)**, stage 10 **(N)**, stage 11 **(O)**, stage 12 **(P)**, and stage 13 **(Q)**. The septum breakage was delayed in the double mutant at stage 12 **(P)**, likely a side effect due to incomplete degeneration of other anther cells. Arrows indicate the persistent middle layer even at stage 12 **(P)**.

Bars in **(A)** to **(C)** = 100 μm; bars in **(D)** to **(F)** = 20 μm; bars in **(G)** to **(I)** = 5 μm; and bars in **(J)** to **(Q)** = 50 μm.

signals appear in the tapetal layer in *rbohe-2* (Figure 6B), indicating delayed tapetal PCD in *rbohe-2*. In contrast with *RBOHE* loss of function, *RBOHE* gain of function resulted in precocious tapetal PCD, as indicated by the appearance of TUNEL-positive signals as early as at stage 9 (Figure 6C). In addition to tapetal cells, TUNEL-positive signals were also visible inside anther locules from degenerating microspores (Figure 6C). These results indicated that *RBOHE* is crucial for the proper timing of tapetal PCD.

RBOHE Loss or Gain of Function Affected Tapetal ROS Levels

The delayed or precocious tapetal PCD by *RBOHE* loss or gain of function suggested the importance of the spatiotemporal production of ROS by NADPH oxidases. To find out whether this was the case, we analyzed anther ROS levels by NBT staining of superoxide anion and 2′,7′-dichlorodihydrofluorescein diacetate (H_2DCF-DA) staining of free radicals. We classified anthers into six groups based on their sizes to categorize anthers at different developmental stages (Supplemental Table 1).

Correlating with the temporal expression of *RBOHE*, developing *Arabidopsis* anthers showed a temporal ROS pattern similar to what has been reported in rice anthers (Hu et al., 2011). The ROS level gradually increased starting from stages 5 and 6, reaching the highest level at approximately stages 8 and 9, and then decreasing until stage 11 (Figure 7; Supplemental Figure 5). By contrast, ROS signals did not show a temporal rise in either *rbohe-2* or *rbohe-2 rhd2-1* (Figure 7A). Both *rbohe-2* and *rbohe-2 rhd2-1* displayed significantly reduced ROS levels during stages 6 to 11 compared with the wild type (Figure 7B). Between *rbohe-2* and *rbohe-2 rhd2-1*, the only significant difference was detected at anther stages 8 and 9 (Figure 7B), suggesting that RHD2 contributes to ROS production mainly during the ROS peak.

In comparison with its loss of function, overexpression of *RBOHE* increased ROS levels significantly around stage 6 (Figure 7A; Supplemental Figure 5) and interfered with the temporal ROS pattern seen in the wild type (Figure 7B). Instead of the ROS peak around stages 8 and 9 in the wild type, *RBOHE* overexpression resulted in relatively uniform ROS levels from stages 6 to 10 (Figure 7B). Considering the significantly increased pollen abortion rates of overexpression lines (Supplemental Figure 4), this result suggests the importance of the spatiotemporal regulation of ROS levels for pollen development.

AMS and MYB80 Regulate *RBOHE* Expression

Anther transcriptomic studies indicated that *RBOHE* was downregulated in *dyt1* and *ams* anthers (Feng et al., 2012) but upregulated in *ms188-1* (an *MYB80* mutant) anthers (Phan et al., 2011),

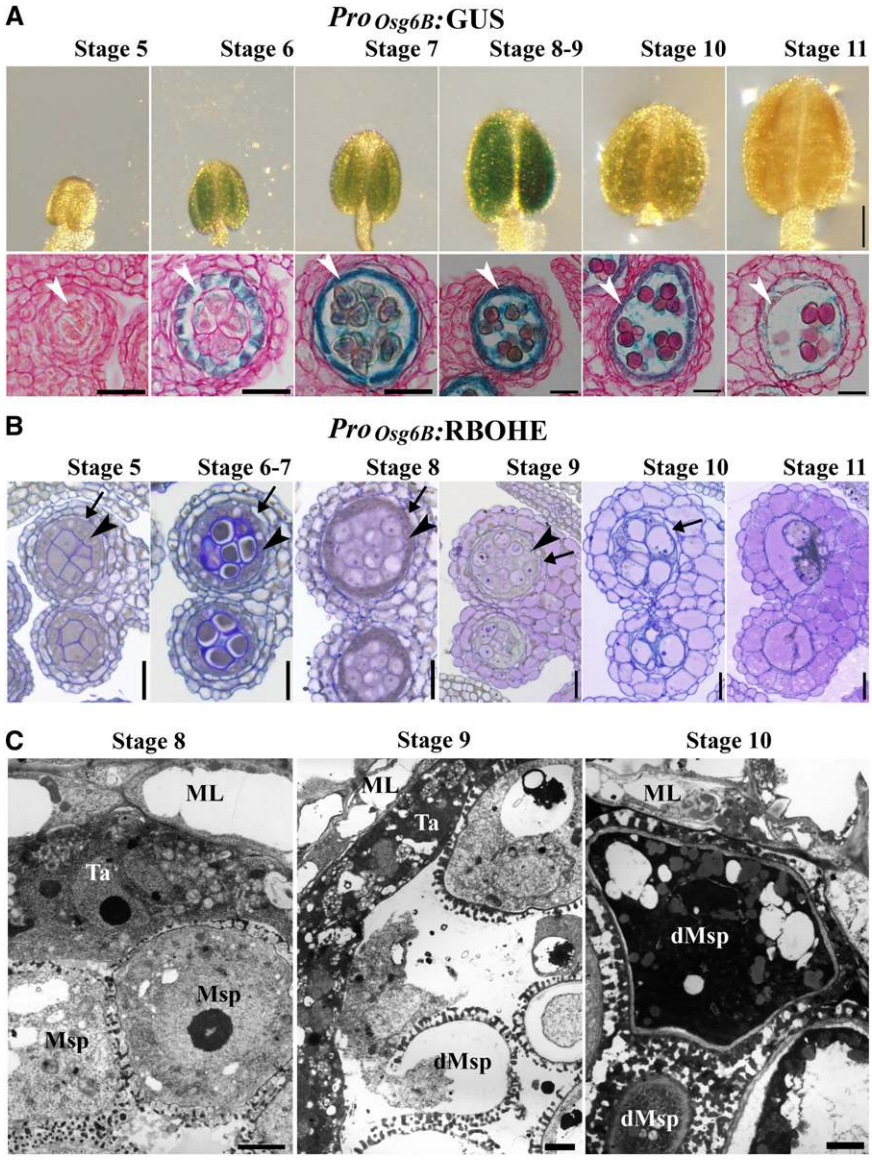

Figure 5. Overexpression of *RBOHE* Resulted in Tapetal Dysfunction.

(A) Histochemical staining analysis of anthers (top) or anther sections (bottom) from the Pro_{Osg6B}:GUS transgenic plants at different developmental stages. Arrowheads point to the tapetal layer. In total, 15 individual Pro_{Osg6B}:GUS transgenic lines were analyzed, and representative images are shown.
(B) Transverse semithin sections of Pro_{Osg6B}:RBOHE anthers at different developmental stages. Arrowheads point to the tapetal layer. Arrows point to the middle layer that persists until late stages in the Pro_{Osg6B}:RBOHE anthers. Three individual Pro_{Osg6B}:RBOHE lines were analyzed, similar results were obtained, and representative images are presented.
(C) Transmission electron micrographs of Pro_{Osg6B}:RBOHE anthers at stages 8, 9, and 10. dMsp, degenerated microspore; ML, middle layer; Msp, microspore; Ta, tapetum.
Bars in **(A)** (anthers) = 100 μm; bars in **(A)** (anther sections) and **(B)** = 20 μm; bars in **(C)** = 2 μm.

suggesting a complex regulatory network by the tapetal transcription factors (Wilson et al., 2001; Parish and Li, 2010; Zhu et al., 2011).

To provide clues to the transcriptional control of the NADPH oxidase–coding genes in the tapetum, we performed in silico analysis on the promoter sequences of *RBOHE* and *RHD2*. *AMS* and *MYB80* are epistatic to *DYT1* and *TDF1* (Zhu et al., 2011). Both have been extensively studied for their *cis*-elements (Xu et al., 2010; Phan et al., 2011). The promoter sequences of *RBOHE* contain four AMS core binding motifs and two MYB80 core binding motifs and the *RHD2* promoter contains two AMS motifs (Supplemental Figure 6), suggesting potential regulation of the NADPH oxidase–coding genes by AMS and MYB80.

Next, we analyzed *RBOHE* expression by histochemical analyses of the Pro_{RBOHE}:GUS reporter lines in the wild type, in

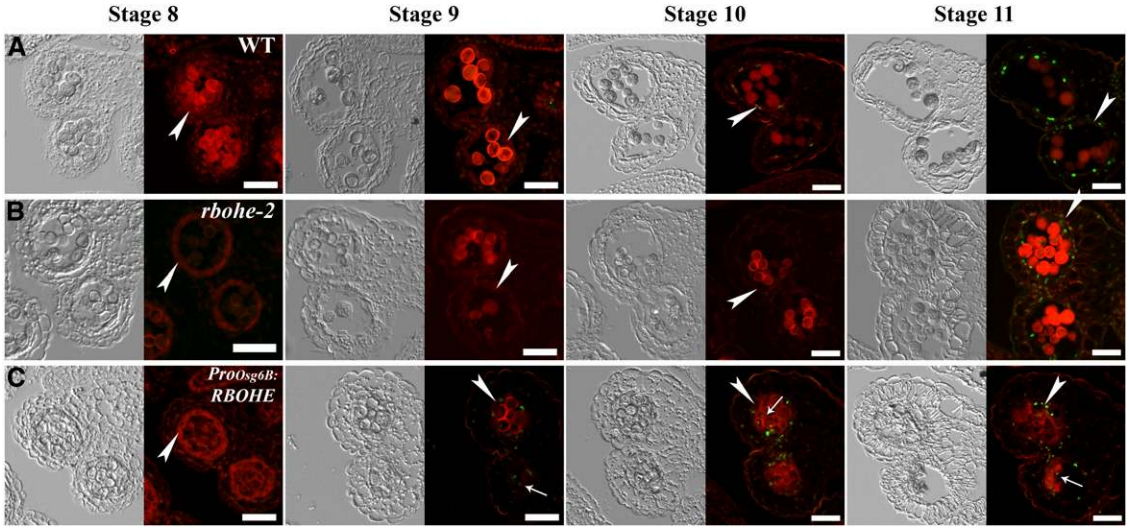

Figure 6. *RBOHE* Loss or Gain of Function Interfered with the Timing of Tapetal PCD.

Fluorescence microscopy of DNA fragmentation detected using the TUNEL assays in sections of wild-type anthers **(A)**, *rbohe-2* anthers **(B)**, and Pro_{Osg6B}:RBOHE anthers **(C)** is shown at different stages. Three individual Pro_{Osg6B}:RBOHE lines were analyzed, similar results were obtained, and representative images are presented. Green fluorescence indicates TUNEL-positive signals, while red fluorescence indicates propidium iodide staining. Corresponding bright-field images are placed together with the fluorescence images. Arrowheads point to the tapetal layer. Arrows in **(C)** indicate TUNEL-positive signals from degenerated microspores that start from stage 9 in Pro_{Osg6B}:RBOHE anthers. Bars = 20 μm.

ams, or in *ms188-1* to examine their potential regulation of the spatiotemporal expression of *RBOHE*. Consistent with the anther transcriptomic data (Phan et al., 2011; Feng et al., 2012), *RBOHE* was reduced in *ams* but enhanced in *ms188-1* (Figure 8A). The transcriptional changes of *RBOHE* were further verified by RNA in situ hybridization using stages 6 and 7 anthers from the wild type, *ams*, or *ms188-1* (Figure 8B). We further used quantitative real-time PCR (qPCR) to measure *RBOHE* expression in wild-type, *ams*, or *ms188-1* anthers at stages 5 to 8 (Figure 8C). We also verified that *RBOHE* was reduced in *dyt1* and *tdf1* by Pro_{RBOHE}:GUS reporter analysis and by RNA in situ hybridization (Supplemental Figure 7). All results demonstrated the different effects of mutations at *AMS* and *MYB80* on *RBOHE* expression (i.e., downregulated in *ams* and upregulated in *ms188-1*), indicating that AMS and MYB80 regulate the transcription of *RBOHE*, directly or indirectly.

Genetic Interaction between *MYB80* and *RBOHE*

The enhanced expression of *RBOHE* in *ms188-1* suggested a negative regulation of *RBOHE* by *MYB80*. Interestingly, we found that *ms188-1* showed elevated ROS levels at early stages of anther development (Supplemental Figure 8), correlating with an enhanced expression of *RBOHE* in *ms188-1* (Figure 8). This result suggested the genetic interaction between *MYB80* and *RBOHE*.

To test this hypothesis, we generated the *ms188-1 rbohe-2* double mutant. Analyses of ROS by either NBT or H_2DCF-DA staining showed that introducing *rbohe-2* into *ms188-1* significantly reduced the ROS level (Supplemental Figure 8), suggesting an epistatic interaction between *RBOHE* and *MYB80* in ROS production.

To gain more insights into their genetic interactions, we performed histological analyses on the *ms188-1 rbohe-2* double mutant. Transverse semithin sections of developing *ms188-1* anthers showed defective tetrad separation and early degeneration of tapetum (Figures 9A and 9C to 9E), as reported (Higginson et al., 2003; Zhang et al., 2007; Phan et al., 2011). Tapetum and microspores degenerated precociously in *ms188-1* (Figures 9A and 9C to 9E). In comparison, microspores degenerated as early in *ms188-1 rbohe-2* (Figure 9F) as in *ms188-1* (Figure 9C). At stages 10 and 11, large amounts of microspores degenerated and anther locules were filled with cell debris, possibly from degenerated microspores in *ms188-1 rbohe-2* (Figures 9G and 9H). However, unlike in *ms188-1*, where tapetal cells fully degenerated at stage 10 (Phan et al., 2011), tapetal cells in *ms188-1 rbohe-2* were still visible at stages 10 and 11 (Figures 9G and 9H), suggesting delayed tapetal degeneration caused by *RBOHE* loss of function.

To find out whether the delayed tapetal degeneration reflected a delayed tapetal PCD process, we performed TUNEL assays on the *ms188-1* single mutant and the *ms188-1 rbohe-2* double mutant. Indeed, unlike the precocious tapetal PCD in *ms188-1* (Figure 10A), TUNEL-positive signals were significantly delayed and reduced in *ms188-1 rbohe-2* (Figure 10B). TUNEL signals were hardly detectable even at stage 11, when other anther tissues started to degenerate (Figure 10B). These results suggested that *RBOHE* was partially epistatic to *MYB80*. In addition, introducing *rbohe-2* into *ms188-1* resulted in a novel phenotype (i.e., much delayed release of microspores from tetrads) (Figures 9B, 9F, and 9G), suggesting a complex rather than a linear interaction between *RBOHE* and *MYB80*.

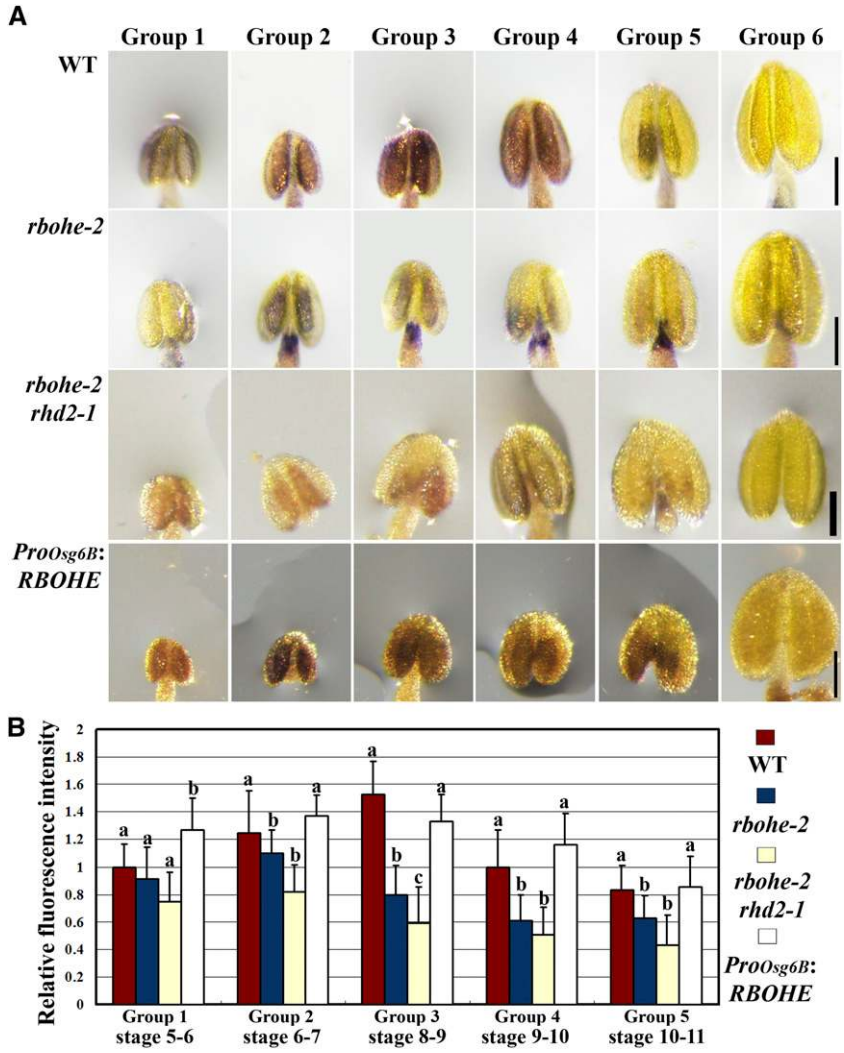

Figure 7. *RBOHE* Loss or Gain of Function Affected Tapetal ROS Levels.

(A) NBT staining analysis of ROS in anthers at various developmental stages from the wild type, *rbohe-2*, *rbohe-2 rhd2-1*, or the Pro_{Osg6B}:RBOHE transgenic plant OX-S1. Classification of anther groups (1 to 6) is based on anther sizes as described in Supplemental Table 1. Bars = 100 μm.
(B) Fluorescence quantification of anther ROS levels by H_2DCF-DA staining of anthers at corresponding stages. ROS signals were hardly detectable in group 6 by H_2DCF-DA staining; thus, they were not quantified. Corresponding anther stages are listed below the group number. Different letters on top of the columns within each group represent significant difference (Student's *t* test, $P < 0.01$).

DISCUSSION

Tapetal NADPH Oxidases Control the Temporal ROS Pattern

ROS can be produced from various subcellular locations, such as chloroplasts, mitochondria, peroxisomes, and apoplast. ROS produced by mitochondrial respiration was especially noted for its roles in metazoan PCD (D'Autréaux and Toledano, 2007). Indeed, failure of ROS scavenging in mitochondria causes wild abortive cytoplasmic male sterility in rice (Luo et al., 2013). However, our results suggest that plasma membrane-localized NADPH oxidases are crucial for the temporal ROS pattern in tapetum.

By using qualitative and quantitative approaches, we show that *Arabidopsis* anthers display a spatiotemporal ROS pattern that reaches its highest level approximately at stages 8 and 9 (Figure 7), during which tapetal degradation commences, to promote microsporogenesis (Sanders et al., 1999; Parish and Li, 2010). Afterward, ROS rapidly decreases to a basal level at stage 11 (Figure 7), when tapetal cells mostly disintegrate (Sanders et al., 1999; Parish and Li, 2010). Similar observations were made in developing anthers in rice (Hu et al., 2011), suggesting the evolutionary conservation of temporal ROS patterns.

Genetic interference with the temporal ROS pattern compromised tapetal degeneration and resulted in pollen abortion (Figures

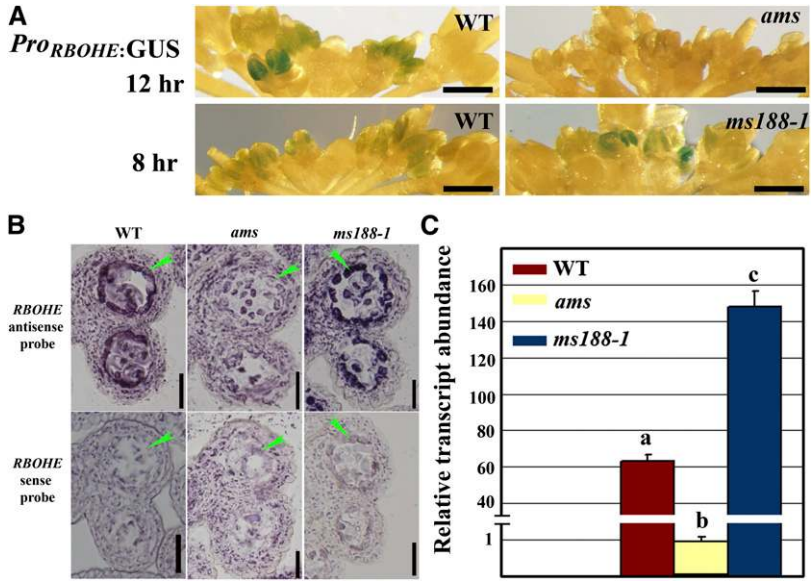

Figure 8. Expression of *RBOHE* Depends on the Tapetal Transcription Factors AMS and MYB80.

(A) Representative histochemical staining of Pro_{RBOHE}:GUS transgenic inflorescences in the wild type, *ams*, and *ms188-1*. The same Pro_{RBOHE}:GUS transgenes were introduced into different genetic backgrounds by crosses for comparison. To highlight differences and avoid signal saturation, a staining duration of 12 or 8 h was used for Pro_{RBOHE}:GUS;*ams* or Pro_{RBOHE}:GUS;*ms188-1*, respectively, to compare with Pro_{RBOHE}:GUS anthers of the same staining protocol. Bars = 500 μm.

(B) In situ analysis of *RBOHE* expression at stages 6 and 7 using an antisense probe in the wild type, *ams*, and *ms188-1*. Anther sections of the wild type, *ams*, and *ms188-1* at the same stage were incubated with a sense probe as a control. Arrowheads point to the tapetal layer. Bars = 50 μm.

(C) qPCR analysis of *RBOHE* expression in wild-type, *ams*, and *ms188-1* anthers at stages 5 to 8. Error bars represent SE. Different letters on top of the columns represent significantly different groups (Student's *t* test, $P < 0.001$).

4 and 5). Specifically, functional loss of *RBOHE* and *RHD2* abolished the ROS peak at stage 8 (Figure 7). However, residual ROS production in the absence of the tapetal NADPH oxidases suggests other tapetal ROS sources, such as mitochondria. Indeed, failure of scavenging mitochondria ROS leads to tapetal dysfunction and pollen abortion in rice (Hu et al., 2011; Luo et al., 2013).

In contrast to the overall reduction of ROS in *RBOHE* loss of function, spatiotemporal overexpression of *RBOHE* significantly enhanced ROS production only at early developmental stages (Figure 7) but not after, even though Pro_{Osg6B}:RBOHE transgenic anthers did show enhanced *RBOHE* expression (Supplemental Figure 4). The discrepancy between the expression of *RBOHE* and ROS levels might be due to posttranslational modifications such as phosphorylation (Marino et al., 2012), *S*-nitrosylation (Yun et al., 2011), Ca^{2+} concentration (Foreman et al., 2003; Ogasawara et al., 2008), binding to phosphatidic acid (Zhang et al., 2009), or protein–protein interaction (Wong et al., 2007), all of which affect NADPH oxidase activities.

Another question regarding NADPH oxidase–mediated spatiotemporal ROS patterns is what results in the transient ROS peak. The differential transcript abundance of NADPH oxidase–coding genes at different anther developmental stages might be one possibility (Figure 1; Supplemental Figure 2). A nonmutually exclusive possibility is temporal expression of ROS scavengers. *ROXY1* and *ROXY2* encode glutaredoxins whose activities at early anther stages may dampen the overall ROS level before stage 8 (Xing and Zachgo, 2008). Alternatively, late expression of ROS scavengers by the tapetal transcription factors, such as MYB80 (Phan et al., 2011), would reduce the overall ROS levels after stage 8, rendering the ROS peak transient.

ROS Generated by NADPH Oxidases May Mediate the Synchronization between Tapetal PCD and Pollen Development

Tapetal cells support pollen development by providing building materials for the pollen wall through PCD at late stages (Wilson and Zhang, 2009; Chang et al., 2011). Although *RBOHE* was also detected in developing microspores at early stages in addition to tapetum during stages 6 to 11 (Figure 1), its gametophytic function, if any, would be negligible because the pollen defect in *RBOHE* loss of function is sporophytic (Supplemental Figure 1). *RBOHE* loss of function resulted in disrupted pollen exine formation (Figure 3) and delayed tapetal PCD (Figure 6), while its gain of function resulted in abnormal deposition of cellular contents in anther locules (Figure 5) and precocious tapetal PCD (Figure 6). Both resulted in significant pollen abortion (Supplemental Figures 1 and 4), providing additional support to the notion that the proper timing of tapetal PCD is critical for pollen development (Higginson et al., 2003; Kawanabe et al., 2006; Li et al., 2011; Phan et al., 2011; Niu et al., 2013).

It has long been accepted that male gametophytes require synchronized development of supporting sporophytic cells. However, the identity of such intercellular signals has remained obscure.

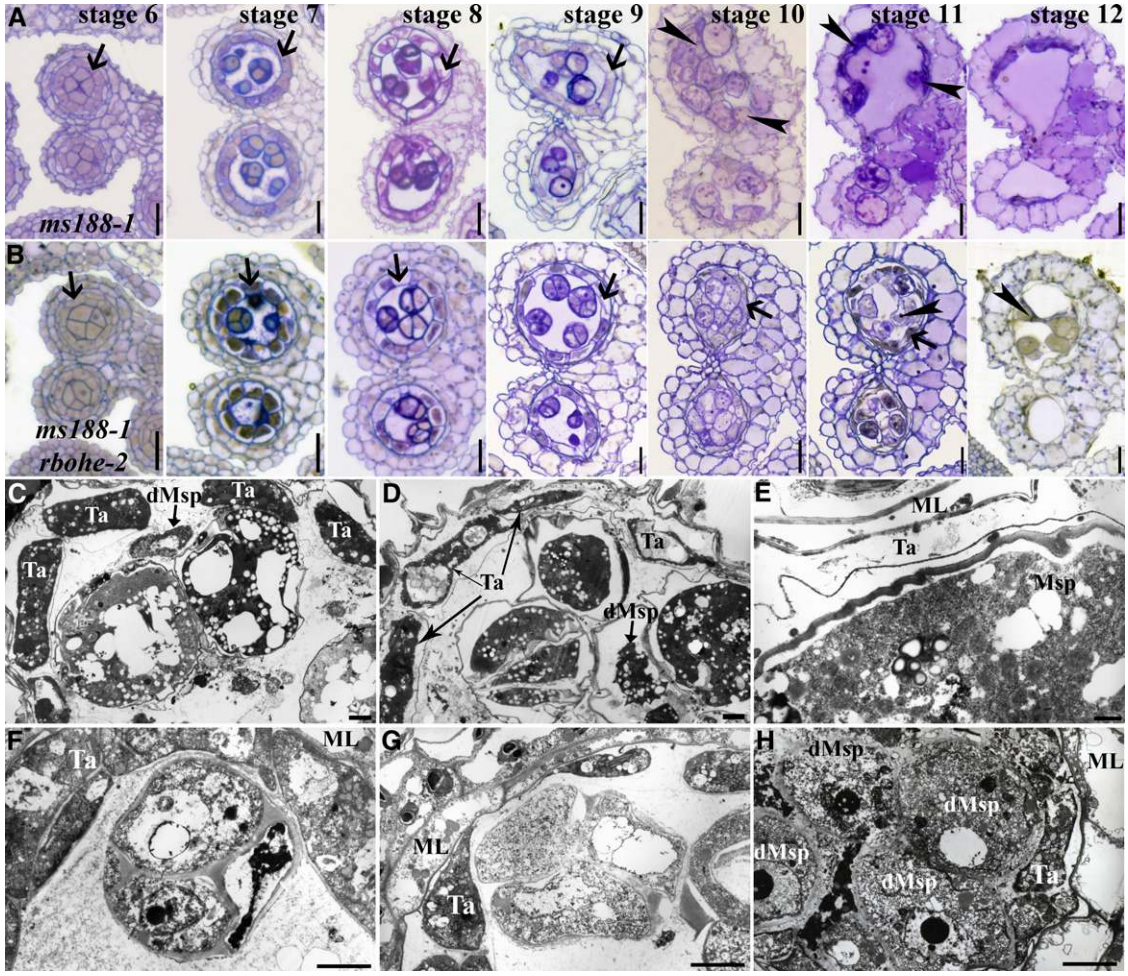

Figure 9. Genetic Interaction between *MYB80* and *RBOHE*.

(A) and **(B)** Transverse semithin sections of *ms188-1* **(A)** and *ms188-1 rbohe-2* **(B)** anthers at different developmental stages.
(C) to **(E)** Transmission electron micrographs of *ms188-1* anthers at stages 8 and 9 **(C)** and stages 9 and 10 (**[D]** and **[E]**). **(E)** shows a closeup at the degenerated tapetum.
(F) to **(H)** Transmission electron micrographs of *ms188-1 rbohe-2* anthers at stages 8 and 9 **(F)**, stages 9 and 10 **(G)**, and stages 10 and 11 **(H)**.
dMsp, degenerated microspore; ML, middle layer; Ta, tapetum. Bars in **(A)** and **(B)** = 20 μm; bars in **(C)** and **(D)** = 1 μm; bars in **(E)** = 500 nm; bars in **(F)** to **(H)** = 2 μm.
[See online article for color version of this figure.]

ROS produced by NADPH oxidases may serve as signaling molecules. The existence of multilevel control of RBOHs, transcriptionally and posttranslationally, makes them good candidates for fine-tuning ROS production in response to extracellular cues, which are essential prerequisites for ROS signal specificity (Mittler et al., 2004, 2011). Apoplastic ROS generated by NADPH oxidases may enter the neighboring microspores to initiate signaling events, leading to developmental synchronization.

ROS are generally not primary agonists but are superimposed cosignals that may allow the integration of cellular activity pathways in accordance with the metabolic state of the cell (D'Autréaux and Toledano, 2007). Well-characterized targets of ROS are redox-sensitive kinases (Neill et al., 2002). ROS also initiate global changes in gene expression through regulating a subset of transcription factors, including MYB family transcription factors (Gechev et al., 2006), to which most components of the transcriptional network belong (Wilson and Zhang, 2009; Parish and Li, 2010; Ma et al., 2012). Indeed, plant PCD processes often involve redox-sensitive transcriptional changes (Swidzinski et al., 2002).

RBOHE and the Tapetal Transcriptional Network

Extensive transcriptomic studies and examination of tapetal mutants have allowed the systematic identification of transcriptional events regulating tapetal PCD, in which *AMS* and *MYB80* act downstream of the transcriptional hierarchy (Wijeratne et al., 2007; Yang et al., 2007; Xu et al., 2010; Phan et al., 2011;

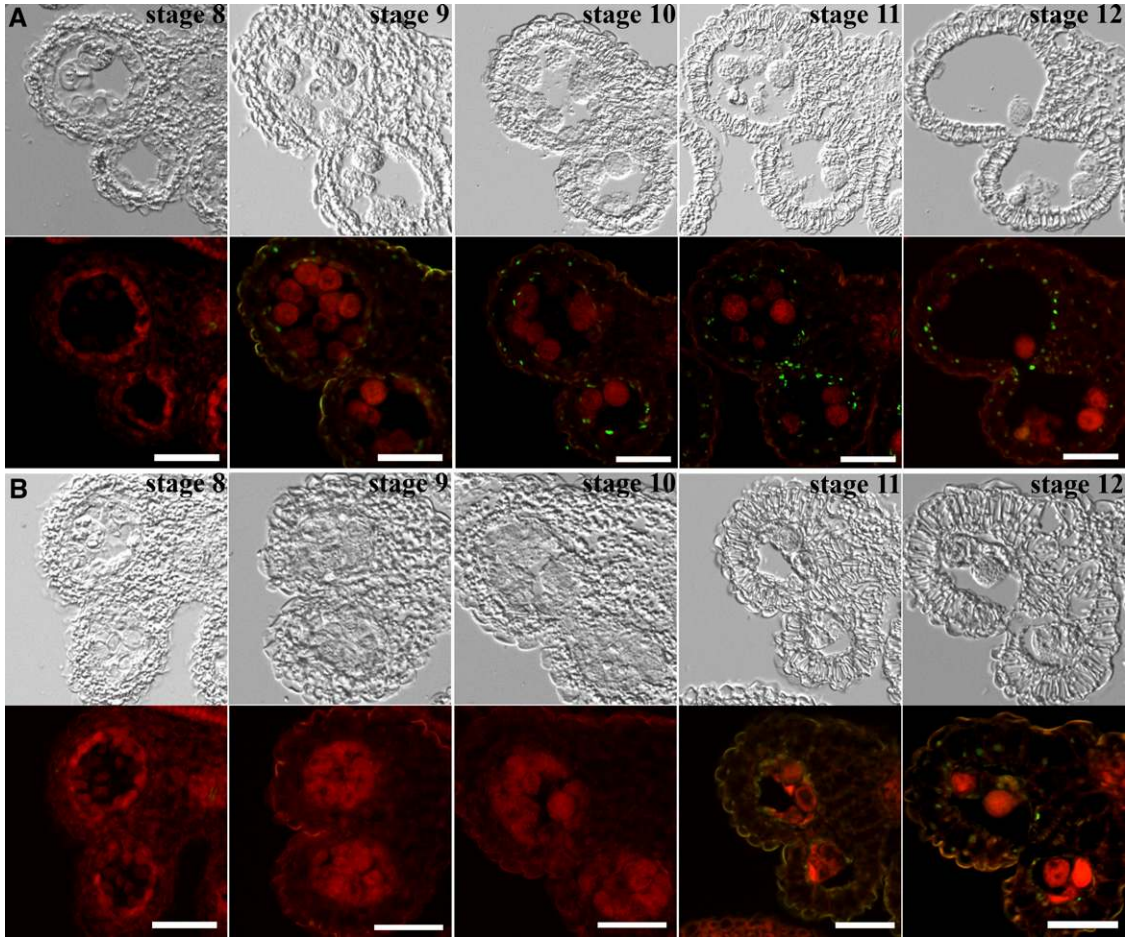

Figure 10. *RBOHE* Is Epistatic to *MYB80* in the Tapetal PCD.

Fluorescence microscopy of DNA fragmentation detected using the TUNEL assays in sections of *ms188-1* **(A)** and *ms188-1 rbohe-2* **(B)** anthers is shown at different developmental stages. Corresponding bright-field images are placed on top of the fluorescence images. Green fluorescence indicates TUNEL-positive signals, and red fluorescence indicates propidium iodide staining. Bars = 20 μm.

Feng et al., 2012; Ma et al., 2012). *RBOHE* was among the genes whose expression was significantly downregulated in *dyt1* and *ams* anthers (Feng et al., 2012) but upregulated in *ms188-1* anthers (Phan et al., 2011), suggesting its transcriptional control by the tapetal transcriptional network (Zhu et al., 2008, 2011), most likely through AMS and MYB80. Indeed, multiple *cis*-elements of AMS and MYB80 are present in the promoter of *RBOHE* (Supplemental Figure 6). By promoter:GUS reporter analysis, RNA in situ hybridization, and qPCR analysis, we confirmed such transcriptional changes of *RBOHE* by mutations at *AMS* and *MYB80* (Figure 8).

We tried to analyze the genetic epistasis between *AMS* and *RBOHE* by introducing Pro_{AMS}:RBOHE into *ams*, but no transgenic lines could be recovered with exogenous *RBOHE* expression in *ams* (H.-T. Xie and Y. Zhang, unpublished data). By contrast, introducing *rbohe-2* into *ms188-1* partially rescued premature tapetal PCD (Figures 9 and 10) and suppressed the high ROS level in *ms188-1* (Supplemental Figure 8), suggesting that *RBOHE* is at least partially epistatic to *MYB80*. However, microspore degeneration still occurred in *ms188-1 rbohe-2* at stages comparable to *ms188-1* (Figures 9 and 10), suggesting the presence of other downstream components of *MYB80* independent of *RBOHE*, possibly genes directly regulated by MYB80 such as *UNDEAD* (Phan et al., 2011).

Both AMS and MYB80 were proposed to function as transcriptional activators (Li et al., 2007; Xu et al., 2010). However, we cannot exclude the possibility that they function as transcriptional repressors of certain genes (Phan et al., 2011). Indeed, MYB80 was proposed to be a bifunctional transcription factor due to the fact that it increases *UNDEAD* expression but decreases *GLOX1* expression, likely through the binding of different cofactors (Phan et al., 2011). The *ams ms188-1* mutants showed similar developmental defects to either *dyt1* or *tdf1* (Zhu et al., 2011), indicating a collaborative action of *AMS* and *MYB80*. However, their antagonistic action on the expression of *RBOHE*, directly or indirectly, suggests a complex rather than additive regulatory mechanism that awaits further investigation.

METHODS

Plant Materials and Growth Conditions

Arabidopsis thaliana plants were grown and transformed as described (Zhou et al., 2013). Growth conditions for *Nicotiana benthamiana* as well as *Agrobacterium tumefaciens*–mediated *RBOHE* expression by infiltration were conducted as described (Wong et al., 2007). The T-DNA insertion lines, SALK_146126C (*rbohe-1*) and SALK_150096C (*rbohe-2*), were obtained from the ABRC (http://www.arabidopsis.org). Columbia-0 was used as the wild type. Transgenic *Arabidopsis* plants were selected on half-strength Murashige and Skoog medium supplemented with either 25 μg/mL hygromycin B or 30 μg/mL glufosinate-ammonium PESTANAL (Sigma-Aldrich). Mutants including *rbohe-1*, *rbohe-2*, and *ams* (SALK_152147) were analyzed by genotyping PCR using the following primers: ZP953/ZP956 for *RBOHE*; ZP2/ZP956 for *rbohe-1/2*; ZP1420/ZP1421 for *AMS*; and ZP1420/ZP2 for *ams*. The single base pair mutation of *rhd2-1* (CAG→CAA) (Foreman et al., 2003) was analyzed using the primers ZP1799/ZP1800 such that PCR products from the wild-type copy but not those from *rhd2-1* can be digested by *Pst*I into 40- and 200-bp fragments. The single base pair mutation of *ms188-1* (CAA→TAA) was characterized by sequencing analyses as described (Zhang et al., 2007). Primers are listed in Supplemental Table 2.

RNA Extraction, RT-PCR, and qPCR

For RT-PCR of *RBOHE* loss-of-function mutants, total RNAs were extracted from inflorescences using the RNeasy plant miniprep kit according to the manufacturer's instructions (Qiagen). For RT-PCR of *RBOHE* gain-of-function lines, total RNAs were extracted from stage 5 to 8 anthers based on the size of floral buds and the position of a given floral bud in an inflorescence as described (Peirson et al., 1996; Phan et al., 2011). Reverse transcription was performed using SuperScript III reverse transcriptase with on-column DNase-I digestion (Invitrogen). Primers used in the RT-PCR were ZP953/ZP955 for the endogenous *RBOHE* and ZP1628/ZP955 for the exogenous *RBOHE*. *Arabidopsis ACTIN2* was used as the internal control for RT-PCR as described (Wang et al., 2013).

For qPCR, total RNAs were extracted from stage 5 to 8 anthers from the wild type, *ams*, or *ms188-1*. The qPCR analysis was performed with the Bio-Rad CFX96 real-time system using SYBR Green real-time PCR master mix (Toyobo) as described (Zhou et al., 2013). Primers ZP2196/ZP2197 were used for *RBOHE*. *GAPDH* and *TUBULIN2* were used as internal controls as described (Zhou et al., 2013). The qPCR was performed using three biological replicates for each genotype, and three technical replicates were conducted for each sample. The data presented in Figure 8 are means of three biological replicates for which three technical replicates were averaged. All primers used in this study are listed in Supplemental Table 2.

Plasmid Construction

All constructs were generated using Gateway technology (Invitrogen). The pENTR/D/TOPO vector (Invitrogen) was used to generate all entry vectors. For GUS reporter constructs, a 2171-bp sequence upstream of the start codon of *RBOHE* was amplified from *Arabidopsis* genomic DNA using the primer pair ZP951/ZP952 to generate the entry vector for Pro_{RBOHE}. A 1634-bp sequence upstream of the start codon of *Osg6B* (Tsuchiya et al., 1994) was amplified from rice (*Oryza sativa* subsp *japonica*) genomic DNA using the primer pair ZP780/ZP781 to generate the entry vector for Pro_{Osg6B}. A 1968-bp sequence upstream of the start codon of *RHD2* was amplified from *Arabidopsis* genomic DNA using the primer pair ZP1041/ZP1042 to generate the entry vector for Pro_{RHD2} (Foreman et al., 2003). Destination vectors for the GUS reporter constructs (i.e., Pro_{RBOHE}:GUS, Pro_{RHD2}:GUS, and Pro_{Osg6B}:GUS) were generated by LR reactions with the corresponding entry vectors and pMD163 (Curtis and Grossniklaus, 2003).

For *RBOHE* expression vectors, the whole genomic fragment of *RBOHE* and the *RBOHE.3* coding sequence were cloned either from genomic DNA or from the anther cDNA library (stages 6 to 10) with the primer pairs ZP953/ZP954 and ZP953/ZP1353, respectively. The gene fragment encoding $RBOHE_{N1\text{-}440}$ was amplified from the anther cDNA library (stages 6 to 10) with the primer pair ZP953/ZP1225. Destination vectors for *RBOHE* overexpression in tapetum were constructed from pH2WG7 (Karimi et al., 2002) by replacing its Pro_{35S} with Pro_{Osg6B} (ZP780/ZP781) and Pro_{AMS} (ZP1284/ZP1285) using the *Sac*I/*Spe*I restriction sites. The corresponding expression vectors, including Pro_{Osg6B}:*RBOHE* and Pro_{AMS}:*RBOHE*, were generated by LR reactions with the *RBOHE* entry vector and corresponding destination vectors using LR Clonase II (Invitrogen). The expression vectors for tobacco (*Nicotiana tabacum*) injection, including Pro_{35S}:RBOHE and Pro_{35S}:$RBOHE_{N1\text{-}440}$, were generated by LR reactions with the corresponding entry vectors and pB7WFG2.0 (Karimi et al., 2002). Primers are listed in Supplemental Table 2.

GUS Histochemistry

Histochemical analysis of GUS activity was performed as described (Zhou et al., 2013). To show the outlines of cells, tissue sections were stained with 100 mg/L ruthenium red (Sigma-Aldrich) for 1 to 2 min before visualization. Images were captured with an Olympus BX51 microscope equipped with a charge-coupled device camera. The histochemical analyses of GUS activity in Pro_{RBOHE}:GUS transgenic plants of different genetic backgrounds (i.e., in *ams*, *ms188-1*, *dyt1*, or *tdf1*) were performed by directly infiltrating anthers with the GUS staining solution under vacuum for 15 min followed by 37°C incubation for 8 or 12 h. Treated samples were subject to decoloration in 95% (v/v) ethanol for 24 to 48 h before being visualized. To ensure comparability, the same Pro_{RBOHE}:GUS transgenes were introduced in different genetic backgrounds and analyzed when the transgene was homozygous. Reproducible results were obtained from three independent experiments.

RNA in Situ Hybridization

RNA in situ hybridization was performed as described (Zhou et al., 2013). Briefly, inflorescences of wild-type or *rbohe-1* plants were fixed in formaldehyde solution (formalin:acetic acid:ethanol:water, 1:2:10:7) overnight at 4°C, embedded in Paraplast (Sigma-Aldrich) after dehydration, and sectioned at 8 μm thickness. The 324-bp fragment specific for *RBOHE* was amplified from the coding region of *RBOHE* with the primer pair ZP1017/ZP1018. A 400-bp fragment specific for *RHD2* was amplified from the coding region of *RHD2* with the primer pair ZP1171/ZP1172. Sense and antisense probes were transcribed in vitro with digoxigenin-UTP by SP6 and T7 RNA polymerases (Roche), respectively. Tissue sections were hybridized with 1.0 ng/μL probes at 42°C overnight in a hybridization solution that contained 50% formamide. Hybridization signals were detected using anti-digoxigenin antibody (Anti-Digoxigenin-Ap Fab fragments; Roche). The samples were observed using an Olympus BX51 microscope.

Pollen Analysis and Anther Staging

Pollen staining with the Alexander dye, scanning electron microscopy of pollen or dehiscing anthers, and pollen in vitro germination were performed as described (Zhou et al., 2013). For pollen abortion rate, pollen grains that have collapsed, lost the normal rugby shape, or have no or disordered apertures are counted as aborted pollen grains. Pollen grains only defective in exine patterns are counted as normal.

For anther staging, because tapetal defects often affect other cell layers, such as delaying microsporogenesis, it is often difficult to

determine anther stages based on either microspore developmental stage or tapetal status (Sanders et al., 1999). Therefore, we determined anther stages based on the size and the position of a given floral bud in an inflorescence as described previously (Peirson et al., 1996). In addition, we also classified anthers of different developmental stages based on anther sizes (width and overall area) as described in Supplemental Table 1.

TUNEL Assay

Whole inflorescences from the wild type, *rbohe-1*, *rbohe-2*, *ms188-1*, *ms188-1 rbohe-2*, and *RBOHE* overexpression lines were processed as described (Phan et al., 2011). In situ nick-end labeling of nuclear DNA fragmentation was performed with the Dead End Fluorometric TUNEL system according to the supplier's instructions (Promega). Samples were analyzed with a confocal laser scanning microscope (Zeiss) using a 488-nm/510-nm excitation/emission spectrum for fluorescein and a 530-nm/640-nm excitation/emission spectrum for propidium iodide as described (Phan et al., 2011).

Histology of Anthers and Histochemical Assays for ROS

Floral buds of different development stages were fixed, embedded, and processed for transverse semithin sections and transmission electron microscopy as described (Wang et al., 2013).

Anthers of various developmental stages were either incubated in 10 mM potassium-citrate buffer (pH 6.0) containing 0.5 mM NBT for superoxide anion detection (Hu et al., 2011) or stained using the fluorescent dye H_2DCF-DA (Sigma-Aldrich) for ROS as described (Huang et al., 2013). For H_2DCF-DA staining, anthers were vacuum infiltrated with 5 μM H_2DCF-DA staining solution for 15 min and then incubated at 25°C for 2 h. Fluorescence imaging of H_2DCF-DA–stained anthers was performed with an Axio Observer D1 microscope equipped with a CCD camera (Zeiss) at the same parameters without reaching signal saturation in any sample for comparative quantification. Anthers were classified into six groups based on their sizes as described in Supplemental Table 1. Three independent experiments were conducted for all genetic backgrounds, and each experiment involved 20 to 25 anthers of a given group. Fluorescence intensity of whole anthers was quantified using ImageJ software (http://rsbweb.nih.gov/ij/).

For NBT staining of tobacco leaves, infiltrated plants were kept in a growth chamber for 2 to 3 d before being examined. Detached leaves were first infiltrated with 0.5 mM NBT solution by vacuum for 15 min followed by 6 h of incubation in 0.5 mM NBT solution. NBT-treated leaves were decolorized in 95% (v/v) ethanol for 48 h before being visualized.

Accession Numbers

Sequence data were archived in TAIR (www.arabidopsis.org) and the National Center for Biotechnology Information with the following accession numbers: *RBOHE* (At1g19230), *RHD2*/*RBOHC* (At5g51060), *AMS* (At2g16910), *MYB80*/*MYB103* (At5g56110), *DYT1* (At4g21330), *TDF1* (At3g28470), and *Osg6B* (Os11g0582400).

Supplemental Data

The following materials are available in the online version of this article.

Supplemental Figure 1. Functional Loss of *RBOHE* Resulted in Sporophytic Male Defects.

Supplemental Figure 2. *RHD2*/*RBOHC* Is Expressed in Tapetum.

Supplemental Figure 3. *RBOHE.3* Encodes an Active NADPH Oxidase.

Supplemental Figure 4. Overexpression of *RBOHE* Disrupted Pollen Development.

Supplemental Figure 5. *RBOHE* Loss or Gain of Function Interfered with Tapetal ROS Levels.

Supplemental Figure 6. The Promoters of *RBOHE* and *RHD2* Contain *cis*-Elements for AMS or MYB80 Binding.

Supplemental Figure 7. Expression of *RBOHE* Was Reduced in *dyt1* and *tdf1*.

Supplemental Figure 8. Genetic Interaction between *MYB80* and *RBOHE* Affects Tapetal ROS Levels.

Supplemental Table 1. Anther Groups Defined for ROS Analyses.

Supplemental Table 2. Oligonucleotides Used in This Study.

ACKNOWLEDGMENTS

We thank Zhong-Nan Yang for the *ams*, *dyt1*, *tdf1*, and *ms188-1* seeds and Lei Ge for the *rhd2-1* seeds. This work was supported by the Major Research Plan from the Ministry of Science and Technology of China (Grant 2013CB945102), by Shandong Provincial Funds for Outstanding Young Scientists (to Y.Z.), and by the Tai-Shan Scholar program from the Shandong Provincial Government (to Y.Z.).

AUTHOR CONTRIBUTIONS

H.-T.X. and Z.-Y.W. performed the experiments. Y.Z., H.-T.X., and S.L. designed the experiments and wrote the article.

Received March 17, 2014; revised April 10, 2014; accepted April 16, 2014; published May 7, 2014.

REFERENCES

Beers, E.P., and McDowell, J.M. (2001). Regulation and execution of programmed cell death in response to pathogens, stress and developmental cues. Curr. Opin. Plant Biol. **4:** 561–567.

Chang, F., Wang, Y., Wang, S., and Ma, H. (2011). Molecular control of microsporogenesis in *Arabidopsis*. Curr. Opin. Plant Biol. **14:** 66–73.

Curtis, M.D., and Grossniklaus, U. (2003). A gateway cloning vector set for high-throughput functional analysis of genes in planta. Plant Physiol. **133:** 462–469.

D'Autréaux, B., and Toledano, M.B. (2007). ROS as signalling molecules: Mechanisms that generate specificity in ROS homeostasis. Nat. Rev. Mol. Cell Biol. **8:** 813–824.

De Pinto, M.C., Locato, V., and De Gara, L. (2012). Redox regulation in plant programmed cell death. Plant Cell Environ. **35:** 234–244.

Feng, B., Lu, D., Ma, X., Peng, Y., Sun, Y., Ning, G., and Ma, H. (2012). Regulation of the Arabidopsis anther transcriptome by DYT1 for pollen development. Plant J. **72:** 612–624.

Foreman, J., Demidchik, V., Bothwell, J.H., Mylona, P., Miedema, H., Torres, M.A., Linstead, P., Costa, S., Brownlee, C., Jones, J. D., Davies, J.M., and Dolan, L. (2003). Reactive oxygen species produced by NADPH oxidase regulate plant cell growth. Nature **422:** 442–446.

Gechev, T.S., Van Breusegem, F., Stone, J.M., Denev, I., and Laloi, C. (2006). Reactive oxygen species as signals that modulate plant stress responses and programmed cell death. Bioessays **28:** 1091–1101.

Higginson, T., Li, S.F., and Parish, R.W. (2003). *AtMYB103* regulates tapetum and trichome development in *Arabidopsis thaliana*. Plant J. **35:** 177–192.

Hsieh, K., and Huang, A.H. (2007). Tapetosomes in *Brassica* tapetum accumulate endoplasmic reticulum–derived flavonoids and alkanes for delivery to the pollen surface. Plant Cell **19:** 582–596.

Hu, L., Liang, W., Yin, C., Cui, X., Zong, J., Wang, X., Hu, J., and Zhang, D. (2011). Rice MADS3 regulates ROS homeostasis during late anther development. Plant Cell **23:** 515–533.

Huang, G.-Q., Li, E., Ge, F.-R., Li, S., Wang, Q., Zhang, C.-Q., and Zhang, Y. (2013). Arabidopsis RopGEF4 and RopGEF10 are important for FERONIA-mediated developmental but not environmental regulation of root hair growth. New Phytol. **200:** 1089–1101.

Ito, T., Nagata, N., Yoshiba, Y., Ohme-Takagi, M., Ma, H., and Shinozaki, K. (2007). *Arabidopsis MALE STERILITY1* encodes a PHD-type transcription factor and regulates pollen and tapetum development. Plant Cell **19:** 3549–3562.

Karimi, M., Inzé, D., and Depicker, A. (2002). GATEWAY vectors for *Agrobacterium*-mediated plant transformation. Trends Plant Sci. **7:** 193–195.

Kawanabe, T., Ariizumi, T., Kawai-Yamada, M., Uchimiya, H., and Toriyama, K. (2006). Abolition of the tapetum suicide program ruins microsporogenesis. Plant Cell Physiol. **47:** 784–787.

Keller, T., Damude, H.G., Werner, D., Doerner, P., Dixon, R.A., and Lamb, C. (1998). A plant homolog of the neutrophil NADPH oxidase gp91^{phox} subunit gene encodes a plasma membrane protein with Ca^{2+} binding motifs. Plant Cell **10:** 255–266.

Kwak, J.M., Mori, I.C., Pei, Z.M., Leonhardt, N., Torres, M.A., Dangl, J.L., Bloom, R.E., Bodde, S., Jones, J.D., and Schroeder, J.I. (2003). NADPH oxidase *AtrbohD* and *AtrbohF* genes function in ROS-dependent ABA signaling in *Arabidopsis*. EMBO J. **22:** 2623–2633.

Lam, E. (2004). Controlled cell death, plant survival and development. Nat. Rev. Mol. Cell Biol. **5:** 305–315.

Lee, Y., Rubio, M.C., Alassimone, J., and Geldner, N. (2013). A mechanism for localized lignin deposition in the endodermis. Cell **153:** 402–412.

Li, H., Yuan, Z., Vizcay-Barrena, G., Yang, C., Liang, W., Zong, J., Wilson, Z.A., and Zhang, D. (2011). *PERSISTENT TAPETAL CELL1* encodes a PHD-finger protein that is required for tapetal cell death and pollen development in rice. Plant Physiol. **156:** 615–630.

Li, N., et al. (2006). The rice *Tapetum Degeneration Retardation* gene is required for tapetum degradation and anther development. Plant Cell **18:** 2999–3014.

Li, S.F., Iacuone, S., and Parish, R.W. (2007). Suppression and restoration of male fertility using a transcription factor. Plant Biotechnol. J. **5:** 297–312.

Luo, D., et al. (2013). A detrimental mitochondrial-nuclear interaction causes cytoplasmic male sterility in rice. Nat. Genet. **45:** 573–577.

Ma, X., Feng, B., and Ma, H. (2012). AMS-dependent and independent regulation of anther transcriptome and comparison with those affected by other *Arabidopsis* anther genes. BMC Plant Biol. **12:** 23.

Marino, D., Dunand, C., Puppo, A., and Pauly, N. (2012). A burst of plant NADPH oxidases. Trends Plant Sci. **17:** 9–15.

Millar, A.A., and Gubler, F. (2005). The *Arabidopsis* GAMYB-like genes, *MYB33* and *MYB65*, are microRNA-regulated genes that redundantly facilitate anther development. Plant Cell **17:** 705–721.

Mittler, R., Vanderauwera, S., Gollery, M., and Van Breusegem, F. (2004). Reactive oxygen gene network of plants. Trends Plant Sci. **9:** 490–498.

Mittler, R., Vanderauwera, S., Suzuki, N., Miller, G., Tognetti, V.B., Vandepoele, K., Gollery, M., Shulaev, V., and Van Breusegem, F. (2011). ROS signaling: The new wave? Trends Plant Sci. **16:** 300–309.

Neill, S., Desikan, R., and Hancock, J. (2002). Hydrogen peroxide signalling. Curr. Opin. Plant Biol. **5:** 388–395.

Niu, N., Liang, W., Yang, X., Jin, W., Wilson, Z.A., Hu, J., and Zhang, D. (2013). EAT1 promotes tapetal cell death by regulating aspartic proteases during male reproductive development in rice. Nat. Commun. **4:** 1445.

Ogasawara, Y., et al. (2008). Synergistic activation of the Arabidopsis NADPH oxidase AtrbohD by Ca^{2+} and phosphorylation. J. Biol. Chem. **283:** 8885–8892.

Parish, R.W., and Li, S.F. (2010). Death of a tapetum: A programme of developmental altruism. Plant Sci. **178:** 73–89.

Peirson, B., Owen, H., Feldmann, K., and Makaroff, C. (1996). Characterization of three male-sterile mutants of *Arabidopsis thaliana* exhibiting alterations in meiosis. Sex. Plant Reprod. **9:** 1–16.

Phan, H.A., Iacuone, S., Li, S.F., and Parish, R.W. (2011). The MYB80 transcription factor is required for pollen development and the regulation of tapetal programmed cell death in *Arabidopsis thaliana*. Plant Cell **23:** 2209–2224.

Phan, H.A., Li, S.F., and Parish, R.W. (2012). MYB80, a regulator of tapetal and pollen development, is functionally conserved in crops. Plant Mol. Biol. **78:** 171–183.

Sanders, P.M., Bui, A.Q., Weterings, K., McIntire, K.N., Hsu, Y.-C., Lee, P.Y., Truong, M.T., Beals, T.P., and Goldberg, R.B. (1999). Anther developmental defects in *Arabidopsis thaliana* male-sterile mutants. Sex. Plant Reprod. **11:** 297–322.

Suzuki, N., Miller, G., Morales, J., Shulaev, V., Torres, M.A., and Mittler, R. (2011). Respiratory burst oxidases: The engines of ROS signaling. Curr. Opin. Plant Biol. **14:** 691–699.

Swidzinski, J.A., Sweetlove, L.J., and Leaver, C.J. (2002). A custom microarray analysis of gene expression during programmed cell death in *Arabidopsis thaliana*. Plant J. **30:** 431–446.

Torres, M.A., and Dangl, J.L. (2005). Functions of the respiratory burst oxidase in biotic interactions, abiotic stress and development. Curr. Opin. Plant Biol. **8:** 397–403.

Torres, M.A., Dangl, J.L., and Jones, J.D. (2002). *Arabidopsis* gp91^{phox} homologues *AtrbohD* and *AtrbohF* are required for accumulation of reactive oxygen intermediates in the plant defense response. Proc. Natl. Acad. Sci. USA **99:** 517–522.

Tsuchiya, T., Toriyama, K., Ejiri, S., and Hinata, K. (1994). Molecular characterization of rice genes specifically expressed in the anther tapetum. Plant Mol. Biol. **26:** 1737–1746.

Vizcay-Barrena, G., and Wilson, Z.A. (2006). Altered tapetal PCD and pollen wall development in the *Arabidopsis ms1* mutant. J. Exp. Bot. **57:** 2709–2717.

Wang, J.G., Li, S., Zhao, X.Y., Zhou, L.Z., Huang, G.Q., Feng, C., and Zhang, Y. (2013). HAPLESS13, the Arabidopsis μ1 adaptin, is essential for protein sorting at the trans-Golgi network/early endosome. Plant Physiol. **162:** 1897–1910.

Wijeratne, A.J., Zhang, W., Sun, Y., Liu, W., Albert, R., Zheng, Z., Oppenheimer, D.G., Zhao, D., and Ma, H. (2007). Differential gene expression in Arabidopsis wild-type and mutant anthers: Insights into anther cell differentiation and regulatory networks. Plant J. **52:** 14–29.

Wilson, Z.A., and Zhang, D.B. (2009). From *Arabidopsis* to rice: Pathways in pollen development. J. Exp. Bot. **60:** 1479–1492.

Wilson, Z.A., Morroll, S.M., Dawson, J., Swarup, R., and Tighe, P.J. (2001). The *Arabidopsis MALE STERILITY1* (*MS1*) gene is a transcriptional regulator of male gametogenesis, with homology to the PHD-finger family of transcription factors. Plant J. **28:** 27–39.

Wong, H.L., Pinontoan, R., Hayashi, K., Tabata, R., Yaeno, T., Hasegawa, K., Kojima, C., Yoshioka, H., Iba, K., Kawasaki, T., and Shimamoto, K. (2007). Regulation of rice NADPH oxidase by binding of Rac GTPase to its N-terminal extension. Plant Cell **19:** 4022–4034.

Xing, S., and Zachgo, S. (2008). *ROXY1* and *ROXY2*, two Arabidopsis glutaredoxin genes, are required for anther development. Plant J. **53:** 790–801.

Xu, J., Yang, C., Yuan, Z., Zhang, D., Gondwe, M.Y., Ding, Z., Liang, W., Zhang, D., and Wilson, Z.A. (2010). The *ABORTED MICROSPORES* regulatory network is required for postmeiotic male reproductive development in *Arabidopsis thaliana*. Plant Cell **22:** 91–107.

Yang, C., Vizcay-Barrena, G., Conner, K., and Wilson, Z.A. (2007). *MALE STERILITY1* is required for tapetal development and pollen wall biosynthesis. Plant Cell **19:** 3530–3548.

Yun, B.W., Feechan, A., Yin, M., Saidi, N.B., Le Bihan, T., Yu, M., Moore, J.W., Kang, J.G., Kwon, E., Spoel, S.H., Pallas, J.A., and Loake, G.J. (2011). S-Nitrosylation of NADPH oxidase regulates cell death in plant immunity. Nature **478:** 264–268.

Zhang, D., Luo, X., and Zhu, L. (2011). Cytological analysis and genetic control of rice anther development. J. Genet. Genomics **38:** 379–390.

Zhang, D.S., Liang, W.Q., Yuan, Z., Li, N., Shi, J., Wang, J., Liu, Y.M., Yu, W.J., and Zhang, D.B. (2008). Tapetum degeneration retardation is critical for aliphatic metabolism and gene regulation during rice pollen development. Mol. Plant **1:** 599–610.

Zhang, W., Sun, Y., Timofejeva, L., Chen, C., Grossniklaus, U., and Ma, H. (2006). Regulation of *Arabidopsis* tapetum development and function by *DYSFUNCTIONAL TAPETUM1* (*DYT1*) encoding a putative bHLH transcription factor. Development **133:** 3085–3095.

Zhang, Y., Zhu, H., Zhang, Q., Li, M., Yan, M., Wang, R., Wang, L., Welti, R., Zhang, W., and Wang, X. (2009). Phospholipase Dα1 and phosphatidic acid regulate NADPH oxidase activity and production of reactive oxygen species in ABA-mediated stomatal closure in *Arabidopsis*. Plant Cell **21:** 2357–2377.

Zhang, Z.B., et al. (2007). Transcription factor *AtMYB103* is required for anther development by regulating tapetum development, callose dissolution and exine formation in Arabidopsis. Plant J. **52:** 528–538.

Zhou, L.Z., Li, S., Feng, Q.N., Zhang, Y.L., Zhao, X., Zeng, Y.L., Wang, H., Jiang, L., and Zhang, Y. (2013). PROTEIN S-ACYL TRANSFERASE10 is critical for development and salt tolerance in *Arabidopsis*. Plant Cell **25:** 1093–1107.

Zhu, J., Chen, H., Li, H., Gao, J.F., Jiang, H., Wang, C., Guan, Y.F., and Yang, Z.N. (2008). *Defective in tapetal development and function 1* is essential for anther development and tapetal function for microspore maturation in Arabidopsis. Plant J. **55:** 266–277.

Zhu, J., Lou, Y., Xu, X., and Yang, Z.N. (2011). A genetic pathway for tapetum development and function in *Arabidopsis*. J. Integr. Plant Biol. **53:** 892–900.